METHOD FOR PREDICTING f_T FOR CARBON NANOTUBE FETs

L.C. Castro†, D.L. John†, *Student Member, IEEE*, D.L. Pulfrey†, *Fellow, IEEE*,
M. Pourfath*, A. Gehring*, *Member, IEEE*, and H. Kosina*, *Member, IEEE*

† Department of Electrical and Computer Engineering, University of British Columbia, Vancouver, BC V6T 1Z4, Canada

* Institute for Microelectronics, Technical University of Vienna, A-1040 Wien, Austria

contact: pulfrey@ece.ubc.ca

ABSTRACT

A method, based on a generic, small-signal equivalent circuit for field-effect transistors, is proposed for predicting the unity-current-gain frequency, f_T, for carbon nanotube devices. The key to the useful implementation of the method is the rigorous estimation of the values for the components of the equivalent circuit. This is achieved by numerical differentiation of the charges and currents resulting from self-consistent solutions to the equations of Schrödinger and Poisson. Sample results are presented which show that f_T can have a very unusual dependence on the gate-source bias voltage. This behaviour is due mainly to the voltage dependence of the transconductance and capacitance in the presence of quasi-bound states in the nanotube.

1 INTRODUCTION

Carbon nanotube field-effect transistors (CNFETs) are being seriously considered for meeting the requirements of the 11 nm technology node [1]. Their DC performance is predicted to be superior to that of ultimately scaled silicon MOSFETs [2, 3], and impressive values for drain current and transconductance have already been reported in prototype devices [4]. The AC capabilities of CNFETs are not yet so obvious. So far, measurements on laboratory devices have been limited by experimental difficulties and parasitics [5, 6, 7]. Thus, the highest reported frequency of 580 MHz, for operation without signal degradation, cannot be viewed as a representative value for an intrinsic device[1]. One way to investigate the AC capabilities of CNFETs would be to perform AC simulations with the same rigour that has characterized earlier DC simulations [9, 10]. This means using a self-consistent Schrödinger-Poisson solver to compute values for the parameters appearing in, for example, a small-signal

[1]Very recently, operation up to 10 GHz has been reported [8], albeit with considerable signal attenuation.

equivalent circuit, from which a useful metric, such as f_T, could be obtained. Through the use of this self-consistent procedure, we expect a more accurate result than that predicted in Ref. [11], where capacitances in the equivalent circuit model were computed assuming a metallic nanotube and electrostatics for an infinitely long coaxial system.

In this paper, we perform a rigorous calculation of the gate-voltage dependencies of both the transconductance [12, 13], and the capacitances, including the so-called "quantum capacitance" [13], in order to compute the small-signal, equivalent-circuit parameters, from which our improved estimates of f_T for CNFETs are obtained. This analysis reveals a bias dependence that is quite unusual, and which may prove useful in voltage-controlled, high-frequency circuitry.

2 THE SMALL-SIGNAL MODEL

2.1 Equivalent circuit

Starting from Maxwell's first two equations, and considering a system with three electrodes, through which charge can enter or leave the system, it follows that

$$\frac{\partial Q}{\partial t} = \frac{\partial Q_S}{\partial t} + \frac{\partial Q_D}{\partial t} + \frac{\partial Q_G}{\partial t} = 0 \, , \tag{1}$$

where Q is the total charge within the system, and Q_S, Q_D, and Q_G refer to charges associated with each of the device's three terminals, namely: the source, drain, and gate, respectively. Labelling displacement currents with a superscript d, it follows from Eq. (1) that

$$i_s^d + i_d^d + i_g^d = 0 \, , \tag{2}$$

where the lower-case subscripts indicate that we are going to be dealing with small-signal parameters. This notation is used also for the voltages, *e.g.*, the total gate voltage v_G comprises a DC voltage V_G and an AC small-signal v_g. If we suppose that Q_S, Q_D, and Q_G are functions of time through the application of time-dependent voltages $v_S(t)$, $v_D(t)$, and $v_G(t)$, then each displacement current will comprise three terms. For example,

$$i_g^d = -C_{GS}\frac{\partial v_S}{\partial t} - C_{GD}\frac{\partial v_D}{\partial t} + C_{GG}\frac{\partial v_G}{\partial t} \, , \tag{3}$$

where the capacitances come from the set

$$C_{ij} = \mp\frac{\partial Q_i}{\partial v_j} \, , \qquad i, j = S, D, G \, , \tag{4}$$

where the minus sign is taken when $i \neq j$, and the plus sign when $i = j$ [14]. Not all the capacitances in this set are independent, and it can be easily shown that, for example,

$$C_{GG} = (C_{GS} + C_{GD}) = (C_{SG} + C_{DG}) \, . \tag{5}$$

Thus, if we now consider v_S and v_D to be held constant, as is appropriate for an estimation of f_T in the absence of parasitic source and drain resistances, then it follows that

$$i_g^d = (C_{SG} + C_{DG}) \frac{\partial v_{GS}}{\partial t} \ . \tag{6}$$

This displacement current, which is also the total gate current i_g, can be computed from an equivalent circuit, such as is shown in Fig. 1.

Turning now to the conduction currents, we employ the standard quasi-static approach for a current that depends on two potential differences, *i.e.*, v_{GS} and v_{DS} in this case. In its linear implementation, this leads to a drain conduction current of

$$i_d^c = g_m v_{gs} + g_{ds} v_{ds} \ . \tag{7}$$

Here, as we are keeping v_{DS} constant, the term involving the output conductance g_{ds} need not be considered.

This completes the specification of the small-signal equivalent circuit. It is a well-founded circuit, with the only approximation being the use of quasi-statics to obtain linear expressions for the conduction currents. Note that the interfacial conductance of $4q^2T/h$, due to transverse-mode reduction on passing from a large, many-mode electrode to a two-mode, quasi-1-D nanotube with a transmission probability T [15], is not shown explicitly in Fig. 1, as it is implicit in the transconductance g_m.

On the basis of the circuit shown in Fig. 1, the common-source, short-circuit, unity-current-gain frequency, as extrapolated from a frequency at which the gain rolls off at $-10\,\text{dB/decade}$, is given by

$$f_T = \frac{g_m}{2\pi(C_{SG} + C_{DG})} \ . \tag{8}$$

2.2 Model parameters

In order to relate C_{SG} and C_{DG} to meaningful physical quantities, firstly we split the charges Q_S and Q_D into two components:

$$\begin{aligned} Q_S &= Q_{SE} + Q_{ST} \ , \\ Q_D &= Q_{DE} + Q_{DT} \ , \end{aligned} \tag{9}$$

where Q_{SE} and Q_{DE} are charges on the actual source and drain electrodes, respectively; and Q_{ST} and Q_{DT} are charges on the nanotube that enter via the source and drain electrodes, respectively. Each of these charges is supplied by the appropriate displacement current, as illustrated in Fig. 2. A capacitance can now be related to each of the charge components.

For the source capacitance, for example, we have

$$C_{SG} = -\frac{\partial Q_S}{\partial v_G} = -\frac{\partial Q_{SE}}{\partial v_G} - \frac{\partial Q_{ST}}{\partial v_G} = C_{SE} + C_{ST} \; . \qquad (10)$$

These capacitive components are readily calculated because their related charges can be computed from a recently described self-consistent, DC, Schrödinger-Poisson solver [9]. This solver has been adapted to employ Neumann boundary conditions at the non-metallic bounding surfaces in the structure depicted in Fig. 2. In our solver, the source- and drain-related nanotube charges, Q_{ST} and Q_{DT}, are computed from integrations of the line charges that are related to the wavefunctions associated with carriers communicating with the system via the source and drain, respectively. Wavefunctions are computed via the effective-mass Schrödinger equation with plane-wave solutions assumed in the metal contacts. A phenomenological band discontinuity is used to model the electrode-nanotube heterointerfaces as simple Schottky barriers. Normalization of the wavefunctions is achieved by setting the probability density current equal to the current expected from the Landauer equation for ballistic transport. The small-signal parameters C_{ST} and C_{DT} are computed for a given drain bias via numerical derivatives with a perturbation in the gate voltage on the order of 0.1 mV. Similarly, g_m is computed from Landauer's equation.

C_{SE} is associated with the change in the charge that resides on the actual source electrode, Q_{SE}. Similarly, C_{DE} is related to a change in Q_{DE}. These charges are computed from appropriate applications of Gauss' Law in integral form.

3 RESULTS AND DISCUSSION

Results are presented for a coaxial transistor structure, as shown in Fig. 2, with Schottky-barrier contacts at the source/tube and drain/tube interfaces. This embodiment, which avoids the need to dope the nanotube, and which employs the ultimate "multi-gate" to combat short-channel effects, is being actively pursued experimentally [16]. Here, by way of an example, we consider a (16,0) carbon nanotube with a radius of 0.63 nm, a length $L_t = 20$ nm, and a relative permittivity of 1 [17]. The insulator has a thickness $T_{\text{ins}} = 2.5$ nm, and its relative permittivity is taken to be 25, as is appropriate for zirconia, which is used in some high-performance CNFETs [18]. The gate electrode is separated from the source and drain electrodes by $L_{sg} = L_{dg} = 4$ nm, and has a thickness $T_g = 3$ nm. The work function of the gate is taken to be the same as that of the intrinsic nanotube (4.5 eV), whereas the source and drain metallizations have a work function of 3.9 eV. Although this

yields an n-type device, inasmuch as the dominant carriers are electrons, p-type operation is directly analogous, and, owing to the symmetry of the nanotube's band-structure about the midgap energy, can be obtained through the use of a higher work function metal. Thus, the CNFET considered here can be classed as a negative-Schottky-barrier device, such as has been predicted to give DC characteristics that are superior to those of devices with either zero- or positive-Schottky barriers at the end contacts [2]. In negative-barrier CNFETs the conduction current is due to thermionic emission at the source-tube and drain-tube interfaces. Quantum-mechanical reflection at these interfaces, due to the band discontinuities mentioned earlier, leads to resonances, and the appearance of quasi-bound states, at least in nanotubes of the short length considered here. This plays a significant role in determining the values for the model parameters discussed below. An illustrative example of the charged quasi-bound states, and the conduction-band profile in the device, is presented in Fig. 3. The example shows charge in the first and second quasi-bound states, and the appearance of charge in an additional quasi-bound state in the potential well at the drain end of the device.

The results presented here are intended to illustrate the ability of the proposed method to provide meaningful estimates of f_T for CNFETs. An optimization of the CNFET structure to suggest an upper bound for f_T is not attempted at this stage, but some comments are offered after the discussion of the present results as to the factors that might be important in this regard. All the results presented below are for operation at $V_{DS} = 0.5\,\mathrm{V}$.

The various components of the capacitance are shown in Fig. 4. Considering, firstly, the tube capacitance C_{ST} due to charge injected from the source, the peak at around $V_{GS} = 0.35\,\mathrm{V}$ corresponds to alignment in energy of the source Fermi level and the first quasi-bound state for electrons in the nanotube [13]. The peak in C_{DT} is displaced from the peak in C_{ST} by approximately V_{DS} [13], and corresponds to alignment in energy of the drain Fermi level and the first quasi-bound state.

Considering now the capacitances associated with changes in charge on the actual end contacts, it can be seen that these are relatively bias-independent. In fact, this is due to C_{SE} and C_{DE} being dominated by the regions of overlap of the end contacts with the edges of the gate electrode. Obviously, this capacitance could be reduced by increasing the separation between the end contacts and the edges of the gate, or by making the gate electrode thinner, or by making the end contacts more "needle-like" [19]. The latter could be achieved by utilizing metallic nanotubes for the source and drain. The total capacitances associated with each electrode are shown in Fig. 5(a).

We now discuss the transconductance, as shown in Fig. 5(b). Firstly, note that the choice of end-contact work function renders the device unipolar, except at very low bias.

Thus, the hole contribution to the transconductance at moderate and high V_{GS} is negligible. Secondly, it can be seen that g_m reaches a maximum, and then decreases as V_{GS} increases. This phenomenon has been reported elsewhere [12, 13]. The overall reduction in g_m at high V_{GS} relates to the increasing electron injection from the drain as the potential energy in the mid-length region of the tube is reduced. The considerable structure in the transconductance plot is due to the presence of the quasi-bound states referred to earlier. As V_{GS} increases, the conduction band edge is pushed below the source Fermi level, and as the quasi-bound states cross this level, g_m increases. Thus, the situation is not dissimilar to that which gives rise to the peaks in capacitance. Indeed, at low temperatures, our simulations reveal that the peaks in transconductance and capacitance do occur at the same biases (see Fig. 6). Evidently, in going from T=4 K to T=300 K, thermal broadening causes peaks that are close together to merge, with the taller one dominating. Thus, the second peak in transconductance dominates the first, while the opposite is true in the capacitance case.

The changes in capacitance and transconductance discussed above lead to a very interesting and unusual bias dependence in the cut-off frequency f_T, as illustrated in Fig. 5(c). For the example of a 20 nm tube, as used here, f_T peaks at about 600 GHz. This is a long way from the value of 4 THz, which can be inferred from a recent model that ignored the bias dependence of the transconductance and capacitances, and attributed the device capacitance to that of an infinite coaxial system, with the quantum capacitance given by that of a metallic, rather than a semiconducting, nanotube [11]. In the finite coaxial system considered here, the mid-tube quantum capacitance is not explicitly identified, as it does not relate to the terminals on which the equivalent circuit is based. It is contained within C_{ST} and C_{DT}, the peak values of which turn out to have comparable magnitudes to the electrostatic electrode capacitances, C_{SE} and C_{DE}, in this particular example; thus, the overall capacitance shows significant bias dependence.

In future work, we will attempt to optimize the Schottky-barrier CNFET as regards high-frequency performance. However, in ending this paper, we can make a few comments regarding the parameters that are likely to be of importance. Clearly, the magnitude of the band discontinuity at the end contacts is significant. We have used a value of -5.5 eV for the depth of the metal conduction band below the Fermi level [9]. Higher values may be appropriate for noble metals of the type that appear suited to end contacts for CNFETs, in which case one can expect more quantum mechanical reflection and a lower transconductance, leading to a reduced f_T. Increasing the barrier height by increasing the work function of the end-contact metal (in the case of n-type devices) will significantly degrade performance because of the appearance of a thick tunneling barrier in the ungated portion of the nanotube.

Changing the nanotube to one of larger bandgap, yet maintaining the barrier height at about $-E_g/2$, may also degrade transconductance, at a given bias, because the ON current can be expected to be smaller, at least at low gate bias. Further, the peaks in transconductance and capacitance will be displaced to higher V_{GS} as more depressing of the conduction-band edge under the gate will be required to align the quasi-bound states with the source Fermi energy. Increasing the ungated regions L_{sg} and L_{dg} should be advantageous in a negative-barrier device because the electrostatic electrode capacitance will be reduced without a degradation in g_m. We have been quite aggressive in the vertical scaling of our device as we have used a high permittivity and a small thickness for the gate insulator. Relaxing these values will not change the resonances, but will shift the peaks in capacitance and transconductance to higher biases, due to the poorer electrostatic coupling between gate and nanotube. Finally, we should mention that in non-Schottky barrier CNFETs, in which the source and drain regions are formed by doping the ungated portions of the nanotube [20, 21], potential wells will form between the end contacts and the intrinsic, gated part of the nanotube, and could lead to resonances somewhat similar to those described here if the doped regions are short enough.

4 CONCLUSIONS

From this work on AC small-signal simulations of Schottky-barrier carbon nanotube field-effect transistors, it can be concluded that:

1. the generic small-signal, equivalent-circuit model for FETs is appropriate for studying the quasi-static AC performance of CNFETs, provided the model parameters are rigorously derived;

2. in the case of short nanotubes with Schottky-barrier end contacts, a resonant structure is formed, leading to the appearance of quasi-bound states;

3. the quasi-bound states lead to gate-bias dependencies of the capacitances and transconductance, which, in turn, give rise to a short-circuit, unity-current-gain frequency f_T which displays a dependence on V_{GS} that is unusual in its oscillatory nature.

Acknowledgement

D.L. Pulfrey sincerely thanks Drs. S. Selberherr and E. Langer for enabling his appointment as a Guest Professor at the Institute of Microelectronics, Technical University of Vienna, during the tenure of which this work was initiated.

References

[1] K. David, "Silicon research at Intel" (2004). [Online.] Available: ftp://download.intel.com/research/silicon/Ken_David_GSF_030604.pdf.

[2] L. C. Castro, D. L. John, and D. L. Pulfrey, "Carbon nanotube transistors: An evaluation," in *Proc. SPIE Conf. Device and Process Technologies for MEMs, Microelectronics, and Photonics III*, vol. 5276, pp. 1–10, 2004. [Online.] Available: http://nano.ece.ubc.ca/pub/publications.htm.

[3] J. Guo, M. Lundstrom, and S. Datta, "Performance projections for ballistic carbon nanotube field-effect transistors," *Appl. Phys. Lett.*, vol. 80, no. 17, pp. 3192–3194, 2002.

[4] A. Javey, J. Guo, Q. Wang, M. Lundstrom, and H. Dai, "Ballistic carbon nanotube field-effect transistors," *Nature*, vol. 424, pp. 654–657, 2003.

[5] D. J. Frank and J. Appenzeller, "High-frequency response in carbon nanotube field-effect transistors," *IEEE Electron Device Lett.*, vol. 25, no. 1, pp. 34–36, 2004.

[6] J. Appenzeller and D. J. Frank, "Frequency dependent characterization of transport properties in carbon nanotube transistors," *Appl. Phys. Lett.*, vol. 84, no. 10, pp. 1771–1773, 2004.

[7] D. V. Singh, K. A. Jenkins, J. Appenzeller, D. Neumayer, A. Gill, and H.-S. P. Wong, "Frequency response of top-gated carbon nanotube field-effect transistors," *IEEE Trans. Nanotechnol.*, vol. 3, no. 3, pp. 383–387, 2004.

[8] X. Huo, M. Zhang, Philip C. H. Chan, Q. Liang, and Z. K. Tang, "High frequency S parameters characterization of back-gate carbon nanotube field-effect transistors," *IEDM Tech. Digest*, 691–694, 2004.

[9] D. L. John, L. C. Castro, P. J. S. Pereira, and D. L. Pulfrey, "A Schrödinger-Poisson solver for modeling carbon nanotube FETs," in *Proc. NSTI Nanotech*, vol. 3, pp. 65–68, March 2004. [Online.] Available: http://nano.ece.ubc.ca/pub/publications.htm.

[10] J. Guo, S. Datta, and M. Lundstrom, "A numerical study of scaling issues for Schottky-barrier carbon nanotube transistors," *IEEE Trans. Electron Devices*, vol. 51, no. 2, pp. 172–177, 2004.

[11] P. J. Burke, "AC performance of nanoelectronics: Towards a ballistic THz nanotube transistor," *Solid-State Electron.*, vol. 48, pp. 1981–1986, 2004.

[12] L. C. Castro, D. L. John, and D. L. Pulfrey, "An improved evaluation of the DC performance of carbon nanotube field-effect transistors," *Nanotechnology*. Accepted August 13, 2004. [Online.] Available: http://nano.ece.ubc.ca/pub/publications.htm.

[13] D. L. John, L. C. Castro, and D. L. Pulfrey, "Quantum capacitance in nanoscale device modeling," *J. Appl. Phys.*, vol. 96, no. 6, pp. 5180–5184, 2004.

[14] Y. P. Tsividis, *Operation and Modeling of the MOS Transistor*, 1st. ed., Chap. 9. New York: McGraw-Hill, 1988.

[15] S. Datta, *Electronic Transport in Mesoscopic Systems*, vol. 3 of *Cambridge Studies in Semiconductor Physics and Microelectronic Engineering*. New York: Cambridge Univ. Press, 1995.

[16] W. Hönlein, F. Kreupl, G. S. Duesberg, A. P. Graham, M. Liebau, R. V. Seidel, and E. Unger, "Carbon nanotube applications in microelectronics," *IEEE Trans. Comp. Packaging Techn.*, vol. 27, no. 4, 629–634, 2004.

[17] F. Léonard and J. Tersoff, "Dielectric response of semiconducting carbon nanotubes," *J. Appl. Phys.*, vol. 81, no. 25, 4835–4837, 2002.

[18] A. Javey, H. Kim, M. Brink, Q. Wang, A. Ural, J. Guo, P. McIntyre, P. McEuen, M. Lundstrom, and H. Dai, "High-κ dielectrics for advanced carbon-nanotube transistors and logic gates," *Nature Materials*, vol. 1, no. 4, 241–246, 2002.

[19] E. Ungersboeck, M. Pourfath, H. Kosina, A. Gehring, B.-Ho Cheong, W.-Jun Park, and S. Selberherr, "Optimization of Single Gate Carbon Nanotube Field Effect Transistors," *IEEE Trans. Nanotechnol.*. Accepted, October, 2004.

[20] A. Javey, R. Tu, D. Farmer, J. Guo, R. Gordon, and H. Dai, "High performance n-type carbon nanotube field-effect transistors with chemically doped contacts," *Nano Lett.*, vol. 5, no. 2, 345–348, 2005.

[21] Yu-Ming Lin, J. Appenzeller, and Ph. Avouris, "Novel carbon nanotube FET design with tunable polarity," *IEDM Tech. Digest*, 687–690, 2004.

List of Figures

1 Small-signal, equivalent circuit for the total AC currents, under the condition that only the potential on the gate is time-dependent. 11

2 Charge supply to and through the source and drain electrodes in a coaxial CNFET. 12

3 Grey-scale representation of the energy- and position-dependence of the electronic charge in the nanotube at $V_{GS} = 0.4\,\mathrm{V}$ and $V_{DS} = 0.5\,\mathrm{V}$. The uniform columns to the left and right represent the energy range below the Fermi level in the source and drain, respectively. The conduction-band edge is superimposed. 13

4 Components of the source and drain capacitances. 14

5 f_T and its components. (a) The total capacitances associated with the source, C_{SG}, and with the drain, C_{DG}; (b) transconductance; (c) f_T. 15

6 Bias dependence, at two temperatures, for (a) capacitance, and (b) transconductance. Note that the peaks in transconductance coincide with peaks in capacitance at the lower temperature. 16

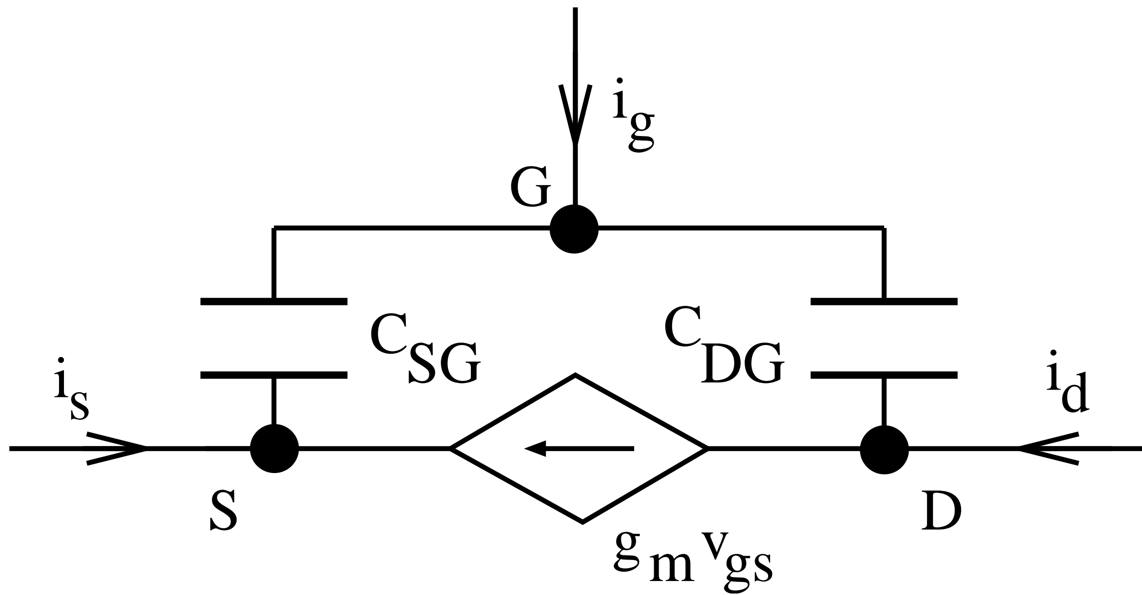

Figure 1: Small-signal, equivalent circuit for the total AC currents, under the condition that only the potential on the gate is time-dependent.

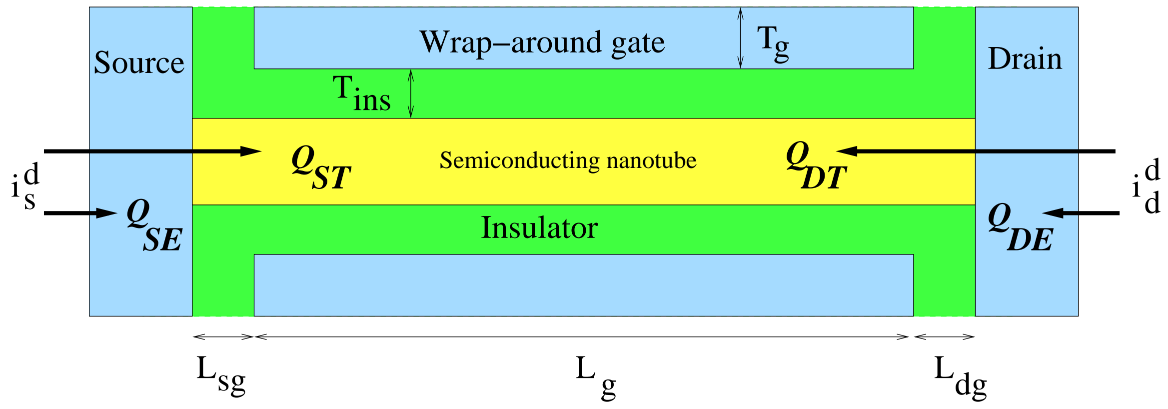

Figure 2: Charge supply to and through the source and drain electrodes in a coaxial CNFET.

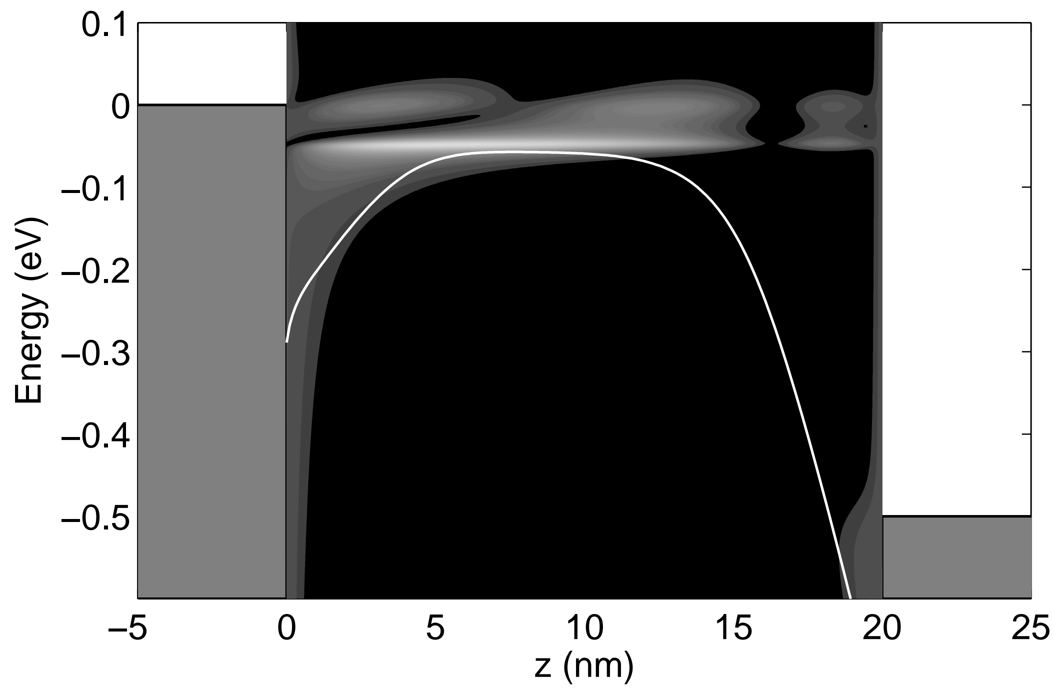

Figure 3: Grey-scale representation of the energy- and position-dependence of the electronic charge in the nanotube at $V_{GS} = 0.4\,\mathrm{V}$ and $V_{DS} = 0.5\,\mathrm{V}$. The uniform columns to the left and right represent the energy range below the Fermi level in the source and drain, respectively. The conduction-band edge is superimposed.

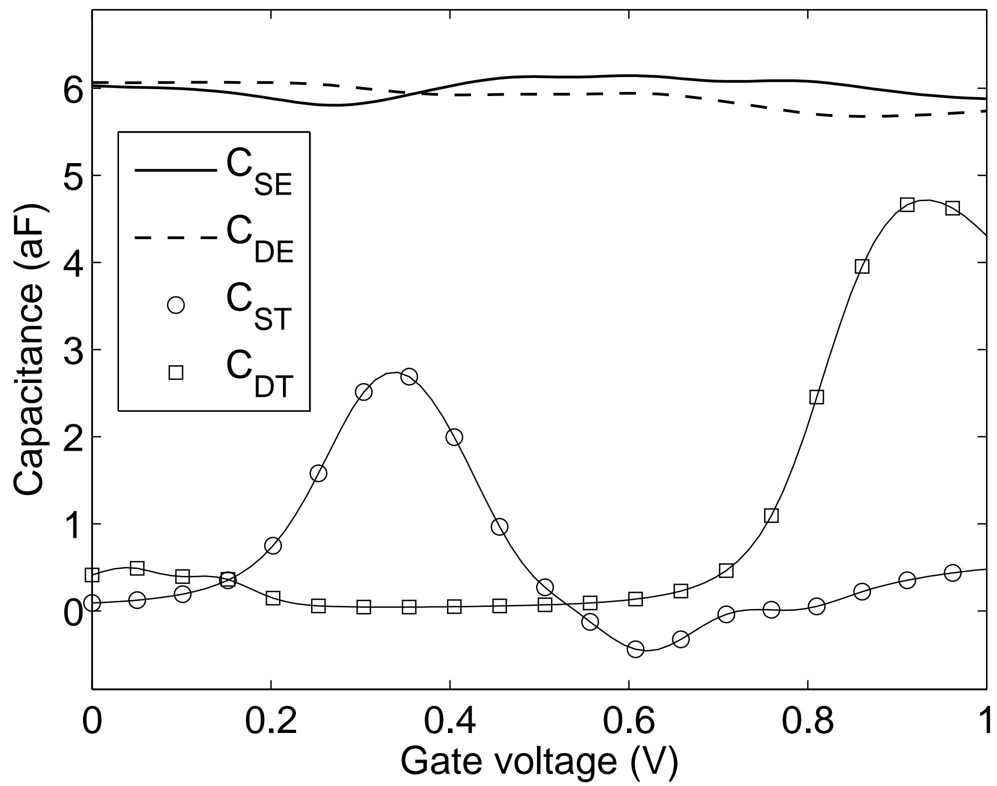

Figure 4: Components of the source and drain capacitances.

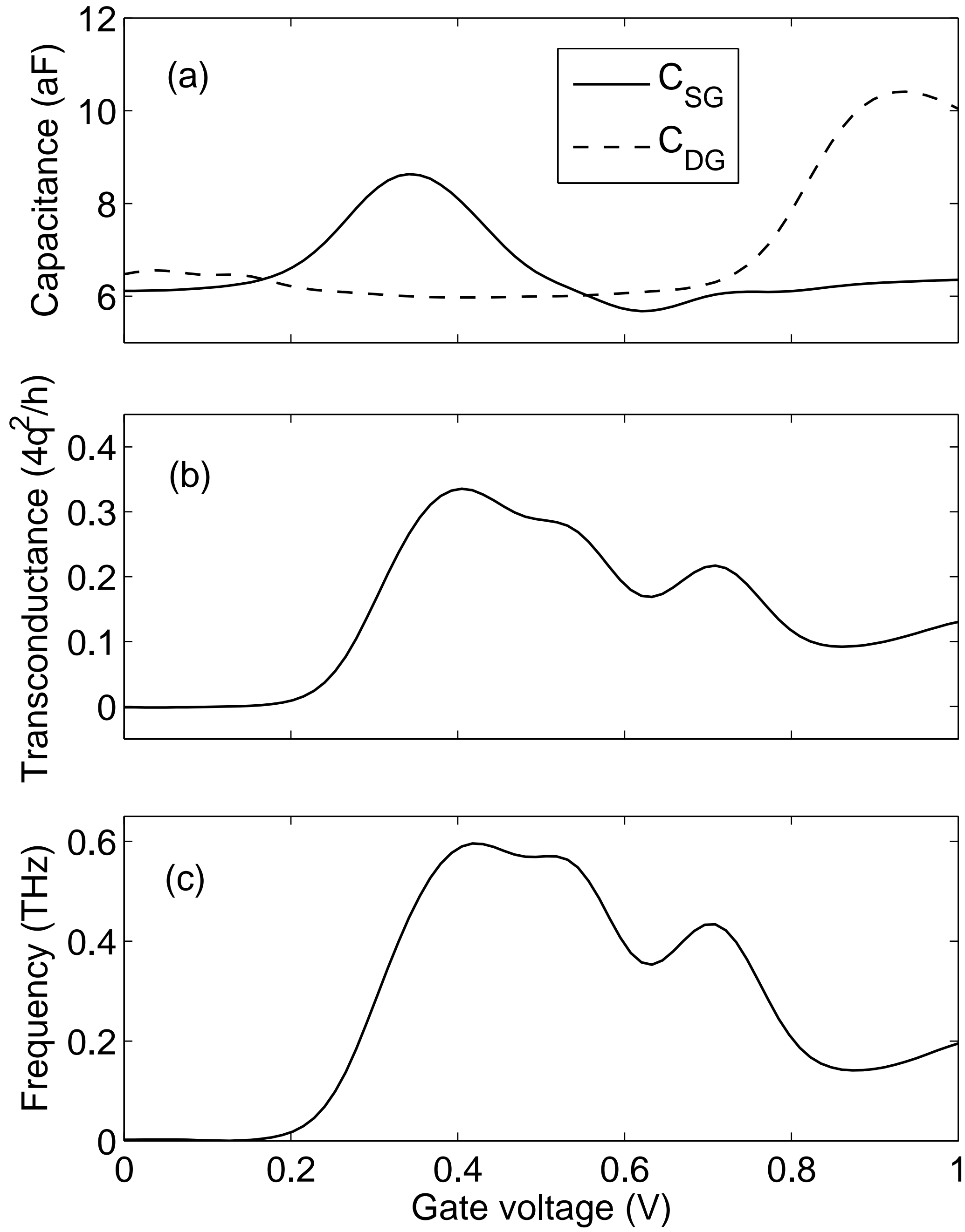

Figure 5: f_T and its components. (a) The total capacitances associated with the source, C_{SG}, and with the drain, C_{DG}; (b) transconductance; (c) f_T.

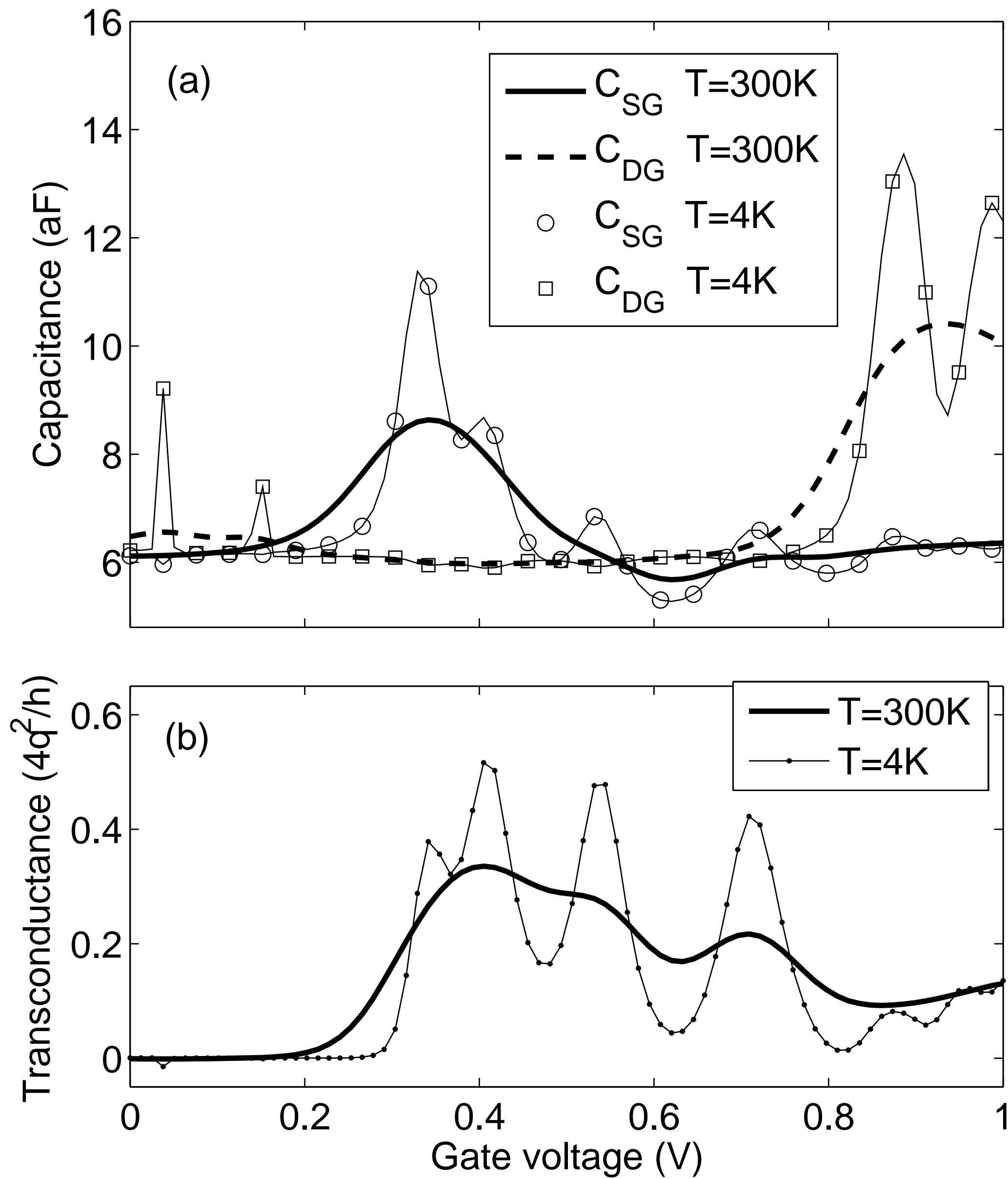

Figure 6: Bias dependence, at two temperatures, for (a) capacitance, and (b) transconductance. Note that the peaks in transconductance coincide with peaks in capacitance at the lower temperature.